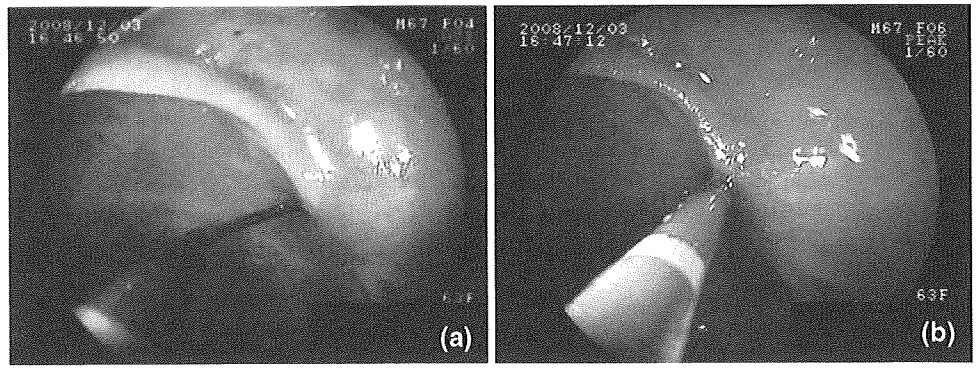

Fig. 5 **a** Guide wire projects slightly from the catheter tip for cannulation. **b** Next, a catheter is inserted following the guide wire

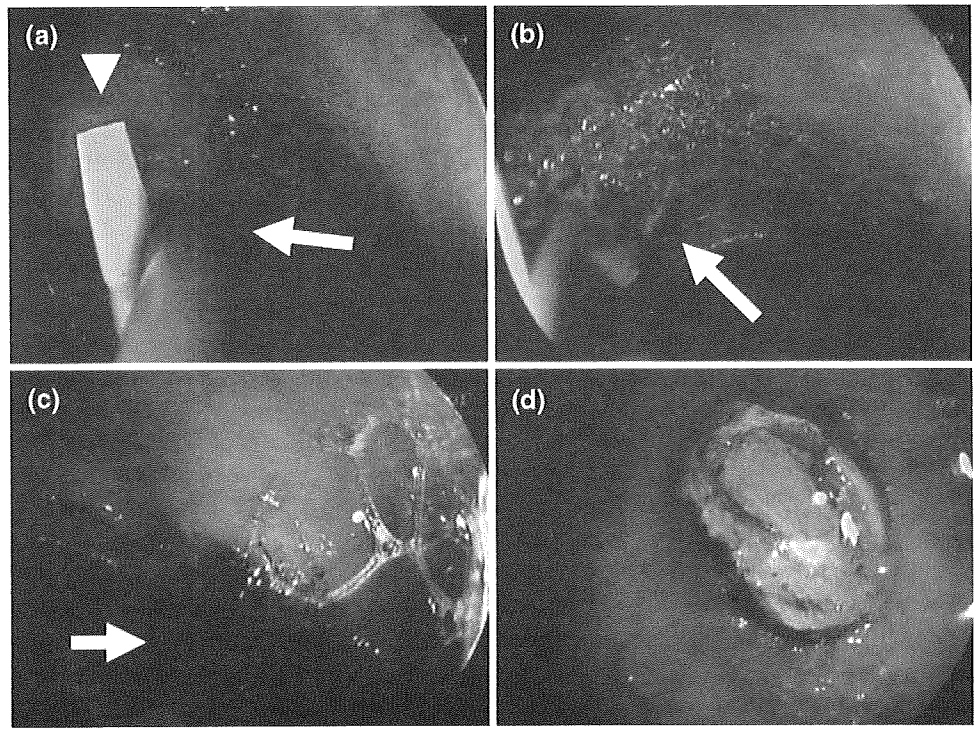

Fig. 6 **a**, **b** A biliary stent was placed in the bile duct (*arrowhead*) and an endoscopic sphincterotomy was performed with a needle knife (*arrow*). **c**, **d** A common bile duct stone was extracted using a mechanical lithotripter (*arrow* in **c**). From Ref. [17], with permission

we use a catheter having a swing tip that can be curved upwardly 85° and downwardly 20° (PR-233Q; Olympus Medical Systems).

Cannulation into the bilio-enteric anastomosis is basically equivalent to cannulation into the papilla of Vater. If the bilio-enteric anastomosis is stenosed, the guide wire is projected slightly from the catheter tip, and after cannulation is performed using the guide wire, the catheter is inserted following the wire (Fig. 5a, b).

Interventions via double-balloon endoscope (DBE)

Previously reported interventions performed after ERCP include balloon dilation for the papilla of Vater or the bilio-enteric anastomosis, sphincterotomy, stone removal using a basket catheter or a balloon catheter, biliary stent placement, and pancreatic stent placement [8–13, 15–17]. Because a DBE has a long working length and a small-diameter working channel, the accessories that can be used are limited, but if accessories are properly selected, many interventions can be performed. Figure 6 shows details of a sphincterotomy performed using a needle knife in order to perform stone removal. After a 7-French biliary stent was placed, an incision was made using a needle knife (KD-441Q; Olympus Medical Systems) in order to expose the biliary stent (Fig. 6a, b). Because the cutting needle was assigned to the biliary stent and the papilla was opened up to expose the biliary stent, safe and successful endoscopic sphincterotomy could be carried out. The biliary stent was removed, and the common bile duct stone was extracted with a mechanical lithotripter (XEMEX Crusher catheter, Zeon Medical, Tokyo, Japan; Fig. 6c, d).

Results

Most previous reports of the use of DBEs for ERCP in patients with a Roux-en-Y anastomosis are small case reports, so it is difficult to state the success rate of the procedure at present. Limiting our scope to published articles that include performance of the procedure in at least five patients [10, 11, 17], the rate of reaching the papilla of Vater or the bilio-enteric anastomosis was 86–94%, and the success rate of ERCP was 67–89%. The rate of reaching the papilla of Vater or the bilio-enteric anastomosis has improved considerably in comparison to results with the use of conventional endoscopes, but the success rate of ERCP is still insufficient. This is largely because DBEs are forward-viewing endoscopes and are not provided with an elevator.

Conclusion

The development of the DBE has made pancreatobiliary endoscopic treatment possible for patients with Roux-en-Y reconstruction in whom an endoscopic approach was conventionally believed to be difficult. However, no standard procedure has yet been established, so it is desirable to accumulate more cases in the future in order to overcome various problems with such endoscopes and other treatment devices, and it is hoped this will lead to further improvements in these endoscopes and devices.

References

1. Hintze RE, Adler A, Veltzke W, Abou-Rebyeh H. Endoscopic access to the papilla of Vater for endoscopic retrograde cholangiopancreatography in patients with Billroth II or Roux-en-Y gastrojejunostomy. Endoscopy. 1997;29:69–73.
2. Wright BE, Cass OW, Freeman ML. ERCP in patients with long-limb Roux-en-Y gastrojejunostomy and intact papilla. Gastrointest Endosc. 2002;56:225–32.
3. Gostout CJ, Bender CE. Cholangiopancreatography, sphincterotomy, and common duct stone removal via Roux-en-Y limb enteroscopy. Gastroenterology. 1988;95:156–63.
4. Elton E, Hanson BL, Qaseem T, Howell DA. Diagnostic and therapeutic ERCP using an enteroscope and a pediatric colonoscope in long-limb surgical bypass patients. Gastrointest Endosc. 1998;47:62–7.
5. Hirai R, Kikuyama M, Sato K, Haruki M, Sakai S, Koide S, et al. An oblique-viewing endoscope with an overtube facilitate bile duct stone removal in Roux-en-Y gastrectomy patients (in Japanese with English abstract). Gastroenterol Endosc. 2006;48:212–6.
6. Yamamoto H, Sekine Y, Sato Y, Higashizawa T, Miyata T, Iino S, et al. Total enteroscopy with a nonsurgical steerable double-balloon method. Gastrointest Endosc. 2001;53:216–20.
7. Yamamoto H, Yano T, Kita H, Sunada K, Ido K, Sugano K. New system of double-balloon enteroscopy for diagnosis and treatment of small intestinal disorders. Gastroenterology. 2003;125:1556–7.
8. Haruta H, Yamamoto H, Mizuta K, Kita Y, Uno T, Egami S, et al. A case of successful enteroscopic balloon dilation for late anastomotic stricture of choledochojejunostomy after living donor liver transplantation. Liver Transpl. 2005;11:1608–10.
9. Spahn TW, Grosse-Thie W, Spies P, Mueller MK. Treatment of choledocholithiasis following Roux-en-Y hepaticojejunostomy using double-balloon endoscopy. Digestion. 2007;75:20–1.
10. Aabakken L, Bretthauer M, Line PD. Double-balloon enteroscopy for endoscopic retrograde cholangiography in patients with a Roux-en-Y anastomosis. Endoscopy. 2007;39:1068–71.
11. Emmett DS, Mallat DB. Double-balloon ERCP in patients who have undergone Roux-en-Y surgery: a case series. Gastrointest Endosc. 2007;66:1038–41.
12. Moreels TG, Roht B, Vandervliet EJ, Parizel PM, Dutré J, Pelckmans PA. The use of the double-balloon enteroscope for endoscopic retrograde cholangiopancreatography and biliary stent placement after Roux-en-Y hepaticojejunostomy. Endoscopy. 2007;39(suppl 1):E196–7.
13. Mönkemüller K, Bellutti M, Neumann H, Malfertheiner P. Therapeutic ERCP with the double-balloon enteroscope in patients with Roux-en-Y anastomosis. Gastrointest Endosc. 2008;67:992–6.
14. Chu YC, Yang CC, Yeh YH, Chen CH, Yueh SK. Double-balloon enteroscopy application in biliary tract disease–its therapeutic and diagnostic functions. Gastrointest Endosc. 2008;68:585–91.
15. Matsushita M, Shimatani M, Takaoka M, Okazaki K. "Short" double-balloon enteroscope for diagnostic and therapeutic ERCP in patients with altered gastrointestinal anatomy. Am J Gastroenterol. 2008;103:3218–9.
16. Koornstra JJ. Double balloon enteroscopy for endoscopic retrograde cholangiopancreaticography after Roux-en-Y reconstruction: case series and review of the literature. Neth J Med. 2008;66:275–9.
17. Ryozawa S, Iwamato S, Urayama N, Iwano H, Harano M, Ishigaki N, et al. Diagnostic and therapeutic endoscopy using a double balloon endoscope in long-limb surgical bypass patients: focusing on ERCP in patients with Roux-en-Y gastrojejunostomy (in Japanese with English abstract). Shokaki Naishikyo (Endoscopia Digestiva). 2007;19:1611–8.
18. Joyce AM, Ahmad NA, Beilstein MC, Kochman ML, Long WB, Baron T, et al. Multicenter comparative trial of the V-scope system for therapeutic ERCP. Endoscopy. 2006;38:713–6.

Hepatology Research 2009; **39**: 648–656 doi: 10.1111/j.1872-034X.2009.00519.x

Original Article

Case–control study for the identification of virological factors associated with fulminant hepatitis B

Atsunori Kusakabe,[1,2] Yasuhito Tanaka,[1] Satoshi Mochida,[3] Nobuaki Nakayama,[3] Kazuaki Inoue,[4] Michio Sata,[5] Norio Isoda,[6] Jong-Hon Kang,[7] Yasukiyo Sumino,[8] Hiroshi Yatsuhashi,[9] Yasuhiro Takikawa,[10] Shuichi Kaneko,[11] Gotaro Yamada,[12] Yoshiyasu Karino,[13] Eiji Tanaka,[14] Junji Kato,[15] Isao Sakaida,[16] Namiki Izumi,[17] Fuminaka Sugauchi,[2] Shunsuke Nojiri,[2] Takashi Joh,[2] Yuzo Miyakawa[18] and Masashi Mizokami[1,19]

[1]Departments of Clinical Molecular Informative Medicine and [2]Gastroenterology and Metabolism, Nagoya City University Graduate School of Medical Sciences, Nagoya, [3]Division of Gastroenterology and Hepatology, Internal Medicine, Saitama Medical University, Saitama, [4]Showa University Fujigaoka Hospital, Yokohama, [5]Kurume University School of Medicine, Kurume, [6]Jichi Medical University, Tochigi, [7]Center for Gastroenterology, Teinekeijinkai Hospital, Sapporo, [8]Toho University Omori Medical Center, Tokyo, [9]National Hospital Organization Nagasaki Medical Center, Nagasaki, [10]Iwate Medical University, Morioka, [11]Department of Signal Transduction, Cancer Research Institute, Kanazawa University, Kanazawa, [12]Kawasaki Hospital, Okayama, [13]Sapporo-Kosei General Hospital, Sapporo, [14]Shinsyu University Graduate School of Medicine, Matsumoto, [15]Sapporo Medical University Hospital, Sapporo, [16]Yamaguchi University Hospital, Ube, [17]Musashino Red Cross Hospital, Musashino, [18]Miyakawa Memorial Research Foundation, Tokyo, and [19]Research Center for Hepatitis and Immunology, International Medical Center of Japan, Kohnodai Hospital, Ichikawa, Japan

Background: Host and viral factors can promote the development of fulminant hepatitis B (FHB), but there have been no case–control studies for figuring out virological parameters that can distinguish FHB.

Methods: In a case–control study, virological factors associated with the development of FHB were sought in 50 patients with FH developed by transient hepatitis B virus (HBV) infection (FH-T) and 50 with acute self-limited hepatitis B (AHB) who were matched for sex and age. In addition, 12 patients with FH developed by acute exacerbation (AE) of asymptomatic HBV carrier (ASC) (FH-C) were also compared with 12 patients without FH by AE of chronic hepatitis B (AE-C).

Results: Higher HBV DNA levels, subgenotype B1/Bj, A1762T/G1764A, G1896A, G1899A and A2339G mutation were significantly more frequent ($P < 0.05$), while hepatitis B e-antigen was less frequent in the FH-T patients than AHB. In multivariate analysis, G1896A mutation (odds ratio [OR], 13.53; 95% confidence interval [CI], 2.75–66.64), serum HBV DNA more than 5.23 log copies/mL (OR, 5.14; 95% CI, 1.10–24.15) and total bilirubin more than 10.35 mg/mL (OR, 7.81; 95% CI, 1.77–34.51) were independently associated with a fulminant outcome by transient HBV infection. On the other hand, in comparison with the patients between FH-C and AE-C groups, there was no significant difference of virological factors associated with the development of FHB.

Conclusion: A number of virological factors have been defined that may distinguish FH-T from AHB in a case–control study. The pathogenic mechanism of FHB between transient HBV infection and AE of ASC would be different.

Key words: acute exacerbation of asymptomatic hepatitis B virus carrier, fulminant hepatitis, genotypes, transient hepatitis B virus infection

INTRODUCTION

IN JAPAN, 634 patients with fulminant hepatitis (FH) were registered from 1998–2003. Of them, 41.8% were infected with hepatitis B virus (HBV) that is the most frequent cause of FH there.[1] HBV is classified into eight genotypes (A–H) based on a sequence divergence of more than 8% in the entire genome of approximately

Correspondence: Dr Yasuhito Tanaka, Department of Clinical Molecular Informative Medicine, Nagoya, City University Graduate School of Medical Sciences, Kawasumi, Mizuho, Nagoya 467-8601, Japan. Email: ytanaka@med.nagoya-cu.ac.jp
Received 22 August 2008; revision 26 January 2009; accepted 24 February 2009.

3200 nucleotides.[2–5] They have distinct geographical distributions and are associated with the severity of liver disease.[6,7] Furthermore, subgenotypes have been reported for HBV/A, B and C, and they are named A1/Aa (Asian/African type) and A2/Ae (European type),[8] B1/Bj (Japanese type) and B2/Ba (Asian type),[9] and C1/Cs (Southeast Asian type) and C2/Ce (East Asian type).[10,11] HBV genotypes/subgenotypes and mutations in the pre-core region and the core promoter can influence the viral replication and expression of hepatitis B e-antigen (HBeAg).[6,12]

Acute HBV infection in adulthood resolves in the most cases by far, but can induce FH or go on to become chronic in some. It has been reported that host and viral factors may influence the development of fulminant hepatitis B (FHB), but the pathogenesis of FHB remains unclear. As for virological factors associated with FHB, mutations in the core promoter (A1762T/G1764A)[13] and the pre-core region (G1896A)[14–16] have been reported in association with the development of FHB in Asia and the Middle East. Additional mutations, including T1753V, T1754V and A2339G in the core gene are implicated, also.[17,18] In regard of HBV genotypes, subgenotype B1/Bj is highly associated with the development of FHB in Japan.[15] In contrast, an association of HBV genotypes with the fulminant outcome has not been reproduced in patients from the USA and Europe.[19–22] Such a discrepancy would be attributed, at least in part, to distinct geographical distributions of HBV genotypes/subgenotypes over the world.

The original definition by Trey *et al.*[23] about fulminant hepatic failure is widely used all over the world. On the other hand, in Japan, the diagnosis of FH was contingent on a slight modification of Trey's original definition by the Inuyama Symposium (Aichi, Japan in 1981). Furthermore, the Intractable Liver Diseases Study Group of Japan modified the criteria for the etiology of FH and late-onset hepatic failure in 2002. According to the criteria of the Intractable Liver Diseases Study Group of Japan, there are two clinical entities of FHB that are induced, respectively, by transient HBV infection and acute exacerbation (AE) of an asymptomatic HBV carrier (ASC).[1]

Recently, FH developing in ASC who undergo AE is increasing in Japan.[1] In patients with hematological malignancy, in particular, rituximab and/or glucocorticoid, can reactivate HBV for the development of FHB.[24] The outcome is poor for FHB precipitating in ASC who undergo acute exacerbation,[1] but it has been difficult to identify it by clinical examinations.

As there have been no case–control studies for figuring out virological parameters that can distinguish FHB, a case–control study was conducted on the patients with FH by transient HBV infection and acute self-limited hepatitis B (AHB) in this study, for the identification of virological factors that influence a fulminant outcome. In addition, the patients with FH by AE of ASC, which is assumed as a different clinical condition from transient HBV infection, were also compared with the patients without FH by AE of chronic hepatitis B (CHB) in a case–control study.

METHODS

Patients

DURING 9 YEARS from 1998 to 2006, in twenty-six hospitals all over Japan, sera were obtained from the 50 FH patients by transient HBV infection (the FH-T group) and the 50 patients with AHB (the AHB group) who were controlled for age and sex. As the elder patients with FHB were enrolled in this study (mean age, 42.8 years), the mean age of AHB patients became relatively high (42.9 years, Table 1). Furthermore, the 12 FH patients developed by AE of ASC (the FH-C group) were also compared with the 12 patients without FH by AE of CHB who were matched by age and sex (the AE-C group).

All the serum samples tested for this study were collected at hospitalization. All 124 patients had hepatitis B surface antigen (HBsAg) in serum. Infection with hepatitis A virus and hepatitis C virus, as well as alcoholic hepatitis, were excluded in them.

The diagnosis of acute hepatitis B was based on sudden manifestation of clinical symptoms of hepatitis and detection of high-titered immunoglobulin (Ig)M anti-hepatitis B core (HBC). Patients with initial high-titered anti-HBC (>90% inhibition by a 1:200 diluted serum) were excluded. The diagnosis of FH was contingent on a slight modification by Inuyama Symposium (Aichi, Japan in 1981) of the original definition by Trey *et al.*:[23] (i) coma of grade II or higher; and (ii) a prothorombin time less than 40% developing within 8 weeks after the onset of hepatitis. To exclude AE of ASC in FH-T and AHB groups, we confirmed the negativity of HBsAg before onset of FHB or AHB and no family histories of hepatitis were found among all the patients. Furthermore, serum HBsAg in all patients with FH-T or AHB became naturally seronegative within 24 weeks. AE of ASC or CHB was defined as the elevation of alanine aminotransferase (ALT >300 IU/L) or total bilirubin (T.bil >3.0 mg/dL).[25] All 24 patients with AE of ASC or CHB could be confirmed positive for serum HBsAg before the onset of acute liver injury.

Table 1 Baseline characteristics between fulminant hepatitis B patients by transient infection (FH-T) and acute self-limited hepatitis B (AHB) patients

Features	FH-T ($n = 50$)	AHB ($n = 50$)	Differences *P*-value
Age (years)	42.8 ± 16.1	42.9 ± 14.6	Matched
Men	25 (50%)	25 (50%)	Matched
ALT (IU/L)	3788 ± 2856	2170 ± 1350	<0.001
AST (IU/L)	3131 ± 3673	1676 ± 1851	<0.05
Total bilirubin (mg/dL)	14.8 ± 8.6	9.5 ± 9.8	<0.01
Prothrombin time (%)	16.9 ± 11.2	72.8 ± 26.0	<0.001
HBeAg positive	15 (30%)	28 (56%)	<0.01
Core protein (log U/mL)	3.21 ± 1.28	3.01 ± 1.00	NS
HBcrAg (log U/mL)	5.30 ± 1.32	5.95 ± 1.13	<0.01
HBV DNA (log copies/mL)	5.97 ± 1.87	4.98 ± 1.17	<0.005
Deceased	19 (38%)	0 (0%)	<0.001

AHB, acute self-limited hepatitis B; ALT, alanine aminotransferase; AST, aspartate aminotransferase; FH-T, fulminant hepatitis B by transient HBV infection; HBcrAg, hepatitis B core related antigen; HBeAg, hepatitis B e antigen; HBV, hepatitis B virus; NS, not significant.

Serological markers of HBV infection

Hepatitis B surface antigen, HBeAg and the corresponding antibody (anti-HBe) were determined by enzyme immunoassay (EIA) (AxSYM; Abbott Japan, Tokyo, Japan) or chemiluminescence enzyme immunoassay (CLEIA) (Fujirebio, Tokyo, Japan). Anti-HBC of IgM and IgG classes were determined by radioimmunoassay (Abbott Japan). Core protein constituting the viral nucleocapsid and HBV core-related antigen (HBcrAg), both of which correlate with HBV DNA in serum, were measured by CLEIA as described elsewhere.[26,27]

Quantification of serum HBV DNA

Hepatitis B virus DNA sequences spanning the S gene were amplified by real-time detection polymerase chain reaction (RTD-PCR) in accordance with the previously described protocol[28] with a slight modification;[8] it has a detection limit of 100 copies/mL.

Sequencing and molecular evolutionary analysis of HBV

Nucleic acids were extracted from serum samples (100 μL) using the QIAamp DNA extraction kit (Qiagen, Hilden, Germany) and subjected to PCR for amplifying genomic areas bearing enhancer II/core promoter/pre-core/core regions [nt 1628–2364], as described previously.[29] The target of PCR covered several mutations which were associated with FHB. Amplicons were sequenced directly with use of the ABI Prism Big Dye ver. 3.0 kit in the AMI 3100 DNA automated sequencer (Applied Biosystems, Foster City, CA, USA). All sequences were analyzed in both forward and backward directions.

Hepatitis B virus genotypes were determined by molecular evolutionary analysis. Reference HBV sequences were retrieved from the DDBJ/EMBL/GenBank database and aligned by CLUSTAL X, then genetic distances were estimated with the 6-parameter method in the Hepatitis Virus Database (http://s2as02.genes.nig.ac.jp/).[30] Based on obtained distances, phylogenetic trees were constructed by the neighbor-joining (NJ) method with the mid-point rooting option. To confirm the reliability of the phylogenetic trees, bootstrap resampling tests were performed 1000 times.

Statistical analysis

Statistical differences were evaluated by the Mann–Whitney *U*-test, Fisher's exact probability test and χ^2-test, where appropriate. Differences were considered to be statistically significant at $P < 0.05$. Multivariate analyses with logistic regression were utilized to sort out independent risk factors for FHB. STATA Software ver. 8.0 was employed for all analyses.

RESULTS

Baseline characteristics of the patients with FHB by transient HBV infection and AHB

TABLE 1 COMPARES baseline clinical characteristics of the 50 FH-T patients and the 50 AHB who

were matched for age and sex. The peak ALT, AST and T.bil levels were significantly higher (3788 ± 2856 vs 2170 ± 1350 IU/L, $P < 0.001$; 3131 ± 3673 vs 1676 ± 1851 IU/L, $P < 0.05$; and 14.8 ± 8.6 vs 9.5 ± 9.8 mg/dL, $P < 0.01$, respectively), while HBeAg was less frequent (30% vs 56%, $P < 0.01$) in the FH-T patients than AHB. The level of HBcrAg was significantly lower (5.30 ± 1.32 vs 5.95 ± 1.13 log U/mL, $P < 0.01$), while HBV DNA loads were higher (5.97 ± 1.87 vs 4.98 ± 1.17 log copies/mL, $P < 0.005$), in the FH-T patients than AHB. The level of core protein in sera tended to be higher in the FH-T patients than AHB (3.21 ± 1.28 vs 3.01 ± 1.00 log U/mL). Death occurred more often in the FH-T patients than AHB (38% vs 0%, $P < 0.001$).

HBV Genotypes and enhancer II/core promoter/pre-core/core Mutations in Patients with FHB by transient HBV infection and AHB

Figure 1(a) compares the distribution of HBV genotypes/subgenotypes between the FH-T and the AHB patients. The subgenotype C2/Ce was most prevalent in both patients with FH-T and AHB (66% and 62%, respectively), whereas B1/Bj was more frequent in the FH-T patients than AHB (22% vs 6%, $P < 0.05$). Likewise, mutations in enhancer II/core promoter/pre-core/core regions are compared between the FH-T and AHB patients in Figure 1(b). A1762T/G1764A, G1896A, G1899A and A2339G mutation were more frequent in the FH-T patients than AHB (48% vs 16%, $P < 0.001$; 62% vs 6%, $P < 0.001$; 24% vs 4%, $P < 0.001$; and 8% vs 0%, $P < 0.05$, respectively).

Figure 2(a) compares various mutations between the 11 FH-T patients and the three AHB patients who were infected with B1/Bj. Only G1896A was significantly more frequent (73% vs 0%, $P < 0.05$), while the lack of any mutations was less common (0% vs 33%, $P < 0.05$) in the FH-T patients than AHB. In comparison with the 33 FH-T patients and the 31 AHB patients who were infected with C2/Ce (Fig. 2b), A1762T/G1764A (70% vs 19%, $P < 0.001$), G1896A (61% vs 6%, $P < 0.001$) and the combination of all three mutations (A1762T/G1764A and G1896A) (45% vs 6%, $P < 0.001$) were significantly more frequent, while the lack of any mutations was less common (9% vs 70%, $P < 0.001$) in the FH-T patients than AHB. Interestingly, all the AHB patients with both G1896A and A1762T/G1764A mutations suffered acute severe hepatitis B that was defined by prothrombin time less than 40% but without coma of grade II or higher.

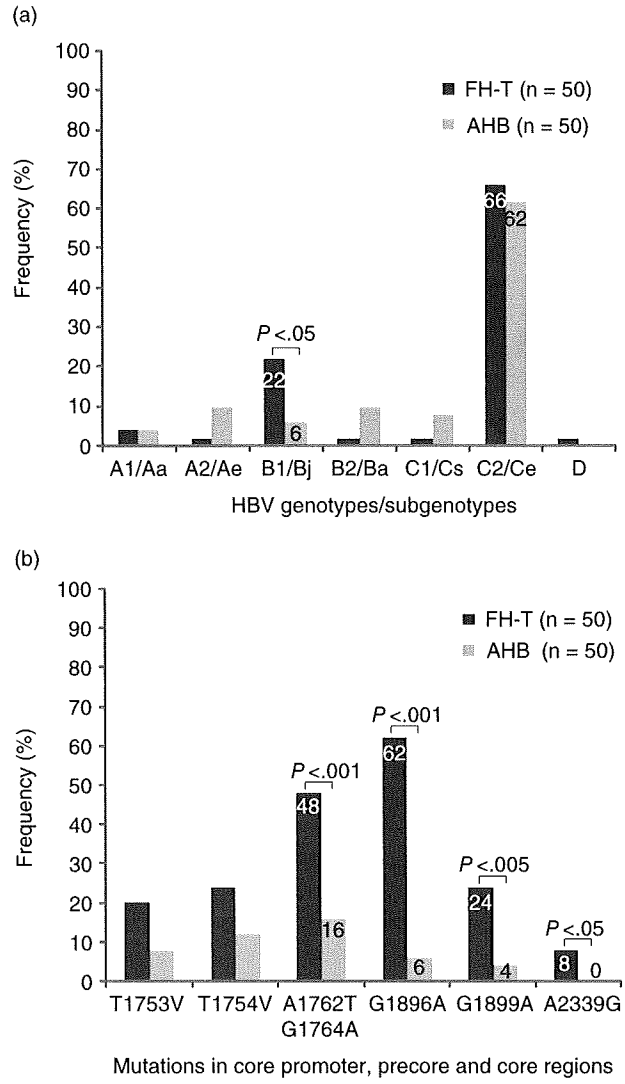

Figure 1 Genotypes/subgenotypes (a) and mutations in core promoter, pre-core and core regions (b) between the 50 transient hepatitis B virus infection (FH-T) and the 50 acute self-limited hepatitis B (AHB) patients.

Factors independently associated with the development of FHB by transient HBV infection

The following independent factors, promoting the development of FHB, were evaluated by multivariate analysis: ALT, AST, T.bil, HBeAg, HBV DNA, core protein, HBcrAg, genotypes/subgenotypes (B1/Bj or not) and mutations (T1753V, T1754V, A1762T/G1764A, G1896A, G1899A and A2339G). T.bil more than 10.35 mg/dL (OR, 7.81 [95% CI, 1.77–34.51], $P = 0.0067$), G1896A mutation (OR, 13.53 [95% CI,

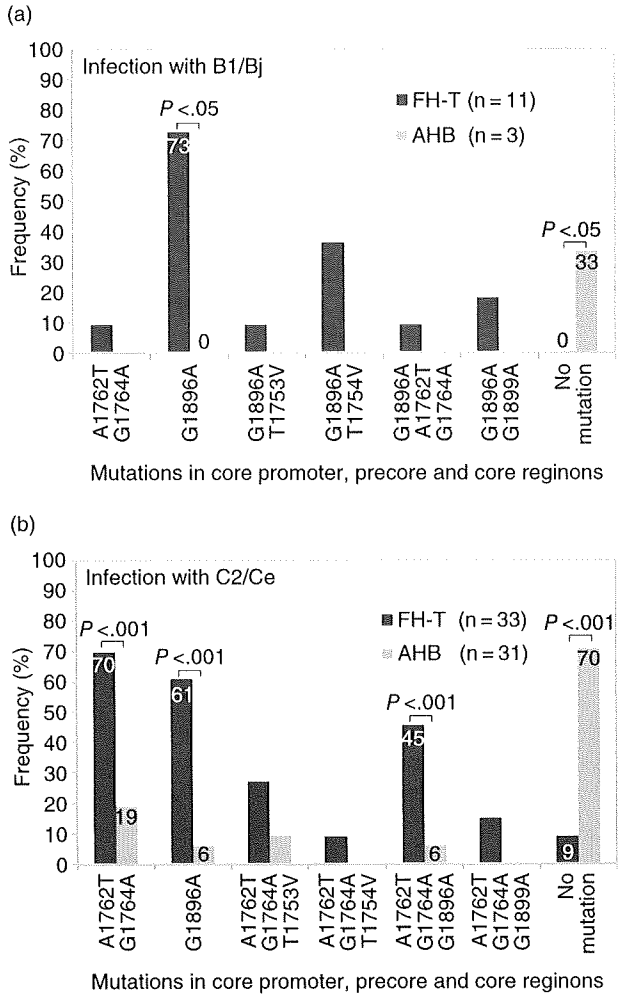

Figure 2 Frequencies of core promoter, pre-core and core mutations compared between the transient hepatitis B virus infection (FH-T) and the acute self-limited hepatitis B (AHB) patients who were infected with HBV of subgenotype B1/Bj (a) or C2/Ce (b).

2.75–66.64], $P = 0.0014$) and serum HBV DNA more than 5.23 log copies/mL (OR, 5.14 [95% CI, 1.10–24.15], $P = 0.0379$) were independent risk factors for the development of FHB by transient HBV infection (Table 2). Other mutations (T1753V, T1754V, A1762T/G1764A, G1899A and A2339G) were not significantly associated with the development of FHB by transient HBV infection, however.

Baseline clinical characteristics for distinguishing between the patients with FHB by AE of ASC (FH-C) and those without FHB by AE of CHB (AE-C)

Table 3 compares baseline clinical characteristics between the 12 FH-C patients and the 12 AE-C patients who were matched for age and sex. The levels of T.bil were significantly higher in the FH-C patients (15.0 ± 7.3 vs 7.3 ± 8.8 mg/dL, $P < 0.05$), but the peak ALT and AST levels tended to be slightly higher in the FH-C patients than AE-C (887 ± 681 vs. 641 ± 620 IU/L and 701 ± 451 vs 601 ± 753 IU/L, respectively). There were also no significant differences in levels of sera HBV DNA, core protein and HBcrAg between these two groups (7.44 ± 1.51 vs 6.60 ± 1.10 log copies/mL, 5.04 ± 1.45 vs 5.07 ± 1.07 log U/mL, and 6.35 ± 1.70 vs 6.29 ± 1.95 log U/mL, respectively).

HBV genotypes and enhancer II/core promoter/pre-core/core mutations between the patients with FH-C and those with AE-C

There were no significant differences in the frequencies of any HBV genotypes between the 12 FH-C patients and the 12 AE-C patients (Fig. 3a). In addition, there were also no significant differences in the frequencies

Table 2 Multivariate analysis for factors independently associated with fulminant hepatitis by transient HBV infection

Factors	Odds ratio	95% confidence interval	*P*-value
Total bilirubin (mg/dL)†			
<10.35	1		
≥10.35	7.81	1.77–34.51	0.0067
G1896A mutation			
Absent	1		
Present	13.53	2.75–66.64	0.0014
HBV DNA (log copies/mL)†			
<5.23	1		
≥5.23	5.14	1.10–24.15	0.0379

†Median values. HBV, hepatitis B virus.

Table 3 Baseline characteristics between patients with FH by AE of ASC (FH-C) and those without FH by AE of CHB (AE-C)

Features	FH-C ($n = 12$)	AE-C ($n = 12$)	Differences *P*-value
Age (years)	51.7 ± 14.7	49.9 ± 5.6	Matched
Male	10 (83%)	9 (75%)	Matched
ALT (IU/L)	887 ± 681	641 ± 620	NS
AST (IU/L)	701 ± 451	601 ± 753	NS
Total bilirubin (mg/dL)	15.0 ± 7.3	7.3 ± 8.8	<0.05
Prothrombin time (%)	25.8 ± 6.6	48.4 ± 21.5	<0.005
HBeAg positive	4 (33%)	3 (25%)	NS
Core protein (log U/mL)	5.04 ± 1.45	5.07 ± 1.07	NS
HBcrAg (log U/mL)	6.35 ± 1.70	6.29 ± 1.95	NS
HBV DNA (log copies/mL)	7.44 ± 1.51	6.60 ± 1.10	NS

AE, acute exacerbation; ALT, alanine aminotransferase; ASC, asymptomatic HBV carrier; AST, aspartate aminotransferase; CHB, chronic hepatitis B; HBcrAg, hepatitis B core related antigen; HBeAg, hepatitis B e antigen; HBV, hepatitis B virus; NS, not significant.

of any specific mutations between these two groups (Fig. 3b).

DISCUSSION

THE MAGNITUDE OF liver injuries depends on the replication level of HBV and cytotoxic immune responses of the host raised against viral epitopes in general.[31] Various viral factors have been proposed that promote the development of FHB, represented by pre-core (G1896A) and core promoter (A1762T/G1764A) mutations.[13–16] Impact of virological factors on the development of FHB has remained controversial, however, especially because these mutations are rarely detected in the patients from the USA and France.[19–21] It has been argued that the development of FHB is not promoted by these mutations and is dependent on host factors including the human leukocyte antigen (HLA) environment.[22]

The expression of HBeAg is terminated by G1896A mutation in the pre-core region at the translation level,[32] and downregulated by the A1762T/G1764A double mutation at the transcription level.[33,34] Lamberts *et al.* are the first to implicate a negative influence of HBeAg on the replication of HBV.[35] Should HBeAg suppress the replication of HBV, presumably by inhibiting the encapsidation of pre-genome,[35] the lack or decrease of HBeAg would enhance the reproduction of HBV. Furthermore, HBeAg acts as a tollerogen to T cells recognizing epitopes on core protein, thereby, obviating immune injury of hepatocytes.[36,37] In the absence or decrease of HBeAg, therefore, hosts would mount vigor cytotoxic T-cell responses to core epitopes excessively presented on hepatocytes, and develop severe liver injuries culminating in FHB.[38]

There is a possibility that influence of viral factors such as HBV mutants with a HBeAg-negative phenotype, on the induction of FHB, may have been confounded by host factors and created disagreement. Therefore, the sheer influence of virological factors on FHB would need to be evaluated in case–control studies, as has been attempted to sort out the influence of HBV genotypes on development of cirrhosis and hepatocellular carcinoma.[8] These backgrounds have instigated us to identify virological factors accelerating the severity of liver disease in the 50 FHB patients by transient HBV infection and the 50 AHB patients who were of the same ethnicity and matched for age as well as sex.

In this case controlled study, A1762T/G1764A, G1896A, G1899A and A2339G mutation were significantly more frequent in the patients with FH-T than AHB, providing further corroboration of previous studies;[13–16] these mutations could enhance viral replication. Interestingly, our recent study using an *in vitro* replication model, showed that A2339G mutation in the core region enhanced viral replication and the effect of A2339G mutation may be associated with inhibition of the cleavage of the core protein by a furin-like protease, resulting in the high expression of the complete core protein.[18] Such enhanced HBV would induce significant immune response, resulting in development of FHB.

In multivariate analysis, higher levels of serum HBV DNA and G1896A mutation were independent virological risk factors for the development of FHB by transient

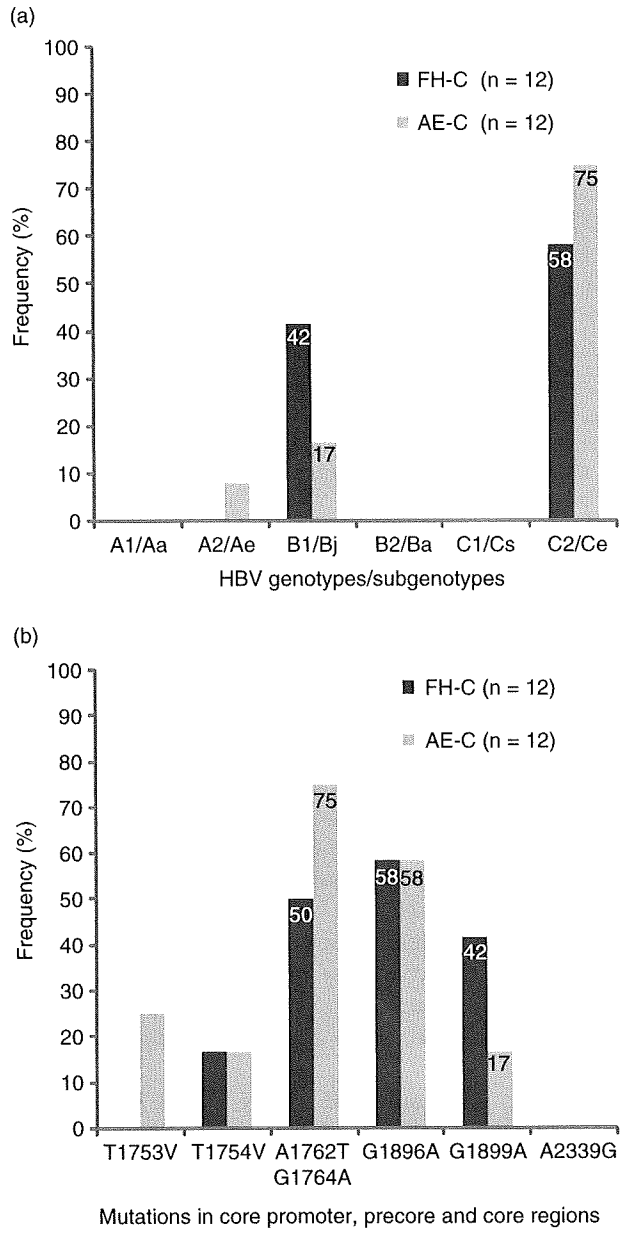

Figure 3 Genotypes/subgenotypes (a) and mutations in core promoter, pre-core and core regions (b) between the 12 transient hepatitis B virus infection (FH-T) and the 12 acute self-limited hepatitis B (AHB) patients.

HBV infection (Table 2). In particular, G1896A mutation was the most important factor associated with the development of FHB. Host responses, represented by T.bil, contributed to the development of FHB as well.

As for HBV genotypes, B1/Bj alone was significantly more frequent in the FH-T patients in univariate analysis. In the patients infected with B1/Bj, G1896A was more frequent in those with FH-T than AHB. In *in vitro* replication analysis, Ozasa *et al.*[15] observed extremely high expressions of intra- and extracellular HBV DNA in culture transfected with an HBV clone of B1/Bj genotype having the G1896A mutation; a high replication would be induced by this pre-core mutation for the induction of FHB. Our clinical results stand in support of this *in vitro* analysis. Taken altogether, chances for developing severe acute or FH would be high in the patients with acute hepatitis who are infected with HBV/B1 having the pre-core mutation. By contrast, in patients infected with C2/Ce, G1896A or A1762T/G1764A, or both was much more frequent in the FH-T patients than AHB. Of note, the co-occurrence of G1896A and A1762T/G1764A mutations was invariably accompanied by either FHB or acute severe hepatitis B in this study. Hence, these pre-core and core-promoter mutations might have addictive or synergetic effects for exacerbating hepatitis, when they emerge in the patients infected with C2/Ce. Such high-risk patients deserve special care and surveillance for signs and symptoms of fulminant or severe acute hepatitis B.

In the present study, serum levels of HBV DNA were significantly higher in the patients with FH-T than AHB. High serum levels of HBV DNA have been reported in patients with FHB;[39] they are followed by rapid decrease as the sequel of virus elimination operated by vigorous immune responses. Because of rapid and extensive elimination of HBV by the host immune system, HBV DNA in serum, in general, has decreased to low levels in patients with FHB at the presentation.[40] HBV DNA levels may be subject to the time that has elapsed from the onset of hepatitis to its measurement.[39] Also, serum levels of core protein (the product of the C gene) closely correlate with serum HBV DNA levels in patients with hepatitis B,[27] and they were compared between the FH-T patients and AHB. The core protein was determined by the newly developed CLEIA method; it is much easier and less expensive than the determination of HBV DNA. The level of core protein has turned out to be marginally higher in the FH-T patients than AHB (Table 1), and therefore might not contribute to an early diagnosis of FHB by transient infection.

Fulminant hepatitis B by AE of ASC is assumed as a different clinical condition from FHB by transient HBV infection. In this study, as there was no case–control study on virological factors associated with FHB for the patients with AE of ASC, we also attempted to identify virological factors associated with the development of FHB in the 12 FH-C and the 12 AE-C patients who were

matched for age as well as sex. Disappointingly, no differences of virological factors such as HBV genotypes and pre-core mutations, which were strongly associated with the development of FHB by transient infection, were found between the FH-C and AE-C patients (Fig. 3a,b). Furthermore, there were also no significant differences about HBeAg-positive rate and the levels of serum HBV DNA or core protein (Table 3), suggesting that several host factors may play a more important role in the development of FHB in ASC instead of virological factors. In this case–control study, however, there seems to be some problems: a small number of patients, different duration of HBV infection, different clinical stage (ASC or CHB) at the onset of AE, and HBV quasispecies complexity. Further investigations are needed to identify factors associated with FHB precipitating in asymptomatic HBV carriers.

In conclusion, virological factors associated with enhancement of viral replication seemed to be important for the development of FHB in the patients by transient HBV infection. But no virological factors were identified for differentiation of the FH-C patients from the AE-C patients. Hence, the pathogenic mechanism of FHB between transient HBV infection and AE of ASC would be different.

ACKNOWLEDGMENTS

WE WOULD LIKE to thank Dr S. Baba, Showa University Hospital, Dr Y. Koga, Kurume University School of Medicine and the other doctors for collecting serum samples in this study. We would also thank Dr N. Maki, Advanced Life Science Institute (Saitama, Japan) for measuring core protein in serum. This study was supported in part by a Grant-in-Aid from the Ministry of Health, Labor and Welfare of Japan, and a Grant-in-Aid from the Ministry of Education, Culture, Sports, Science and Technology.

REFERENCES

1 Fujiwara K, Mochida S, Matsui A, Nakayama N, Nagoshi S, Toda G. Fulminant hepatitis and late onset hepatic failure in Japan. *Hepatol Res* 2008; **38**: 646–57.
2 Norder H, Hammas B, Lofdahl S, Courouce AM, Magnius LO. Comparison of the amino acid sequences of nine different serotypes of hepatitis B surface antigen and genomic classification of the corresponding hepatitis B virus strains. *J Gen Virol* 1992; **73** (Pt 5): 1201–8.
3 Okamoto H, Tsuda F, Sakugawa H *et al.* Typing hepatitis B virus by homology in nucleotide sequence: comparison of surface antigen subtypes. *J Gen Virol* 1988; **69**: 2575–83.
4 Stuyver L, De Gendt S, Van Geyt C *et al.* A new genotype of hepatitis B virus: complete genome and phylogenetic relatedness. *J Gen Virol* 2000; **81** (Pt 1): 67–74.
5 Arauz-Ruiz P, Norder H, Robertson BH, Magnius LO. Genotype H: a new Amerindian genotype of hepatitis B virus revealed in Central America. *J Gen Virol* 2002; **83** (Pt 8): 2059–73.
6 Miyakawa Y, Mizokami M. Classifying hepatitis B virus genotypes. *Intervirology* 2003; **46**: 329–38.
7 Chu CJ, Lok AS. Clinical significance of hepatitis B virus genotypes. *Hepatology* 2002; **35**: 1274–6.
8 Tanaka Y, Hasegawa I, Kato T *et al.* A case-control study for differences among hepatitis B virus infections of genotypes A (subtypes Aa and Ae) and D. *Hepatology* 2004; **40**: 747–55.
9 Sugauchi F, Orito E, Ichida T *et al.* Hepatitis B virus of genotype B with or without recombination with genotype C over the pre-core region plus the core gene. *J Virol* 2002; **76**: 5985–92.
10 Huy TT, Ushijima H, Quang VX *et al.* Genotype C of hepatitis B virus can be classified into at least two subgroups. *J Gen Virol* 2004; **85** (Pt 2): 283–92.
11 Tanaka Y, Orito E, Yuen MF *et al.* Two subtypes (subgenotypes) of hepatitis B virus genotype C: a novel subtyping assay based on restriction fragment length polymorphism. *Hepatol Res* 2005; **33**: 216–24.
12 Lindh M, Andersson AS, Gusdal A. Genotypes, nt 1858 variants, and geographic origin of hepatitis B virus–large-scale analysis using a new genotyping method. *J Infect Dis* 1997; **175**: 1285–93.
13 Sato S, Suzuki K, Akahane Y *et al.* Hepatitis B virus strains with mutations in the core promoter in patients with fulminant hepatitis. *Ann Intern Med* 1995; **122**: 241–8.
14 Omata M, Ehata T, Yokosuka O, Hosoda K, Ohto M. Mutations in the pre-core region of hepatitis B virus DNA in patients with fulminant and severe hepatitis. *N Engl J Med* 1991; **324**: 1699–704.
15 Ozasa A, Tanaka Y, Orito E *et al.* Influence of genotypes and pre-core mutations on fulminant or chronic outcome of acute hepatitis B virus infection. *Hepatology* 2006; **44**: 326–34.
16 Liang TJ, Hasegawa K, Rimon N, Wands JR, Ben-Porath E. A hepatitis B virus mutant associated with an epidemic of fulminant hepatitis. *N Engl J Med* 1991; **324**: 1705–9.
17 Imamura T, Yokosuka O, Kurihara T *et al.* Distribution of hepatitis B viral genotypes and mutations in the core promoter and pre-core regions in acute forms of liver disease in patients from Chiba, Japan. *Gut* 2003; **52**: 1630–7.
18 Sugiyama M, Tanaka Y, Kurbanov F, Nakayama N, Mochida S, Mizokami M. Influences on hepatitis B virus replication by a naturally occurring mutation in the core gene. *Virology* 2007; **365**: 285–91.

19 Laskus T, Persing DH, Nowicki MJ, Mosley JW, Rakela J. Nucleotide sequence analysis of the pre-core region in patients with fulminant hepatitis B in the United States. *Gastroenterology* 1993; **105**: 1173–8.
20 Liang TJ, Hasegawa K, Munoz SJ *et al.* Hepatitis B virus pre-core mutation and fulminant hepatitis in the United States. A polymerase chain reaction-based assay for the detection of specific mutation. *J Clin Invest* 1994; **93**: 550–5.
21 Feray C, Gigou M, Samuel D, Bernuau J, Bismuth H, Brechot C. Low prevalence of pre-core mutations in hepatitis B virus DNA in fulminant hepatitis type B in France. *J Hepatol* 1993; **18**: 119–22.
22 Karayiannis P, Alexopoulou A, Hadziyannis S *et al.* Fulminant hepatitis associated with hepatitis B virus e antigen-negative infection: importance of host factors. *Hepatology* 1995; **22**: 1628–34.
23 Trey C, Lipworth L, Chalmers TC *et al.* Fulminant hepatic failure. Presumable contribution to halothane. *N Engl J Med* 1968; **279**: 798–801.
24 Ng HJ, Lim LC. Fulminant hepatitis B virus reactivation with concomitant listeriosis after fludarabine and rituximab therapy: case report. *Ann Hematol* 2001; **80**: 549–52.
25 Fujiwara K, Mochida S, Matsui A. [Prospective study for the efficiency of lamivudine for the patients with acute exacerbation of HBV carrier.] *Annual Report of Intractable Liver Disease Study Group of Japan, the Ministry of Health, Welfare and Labor* 2004. (In Japanese.)
26 Kimura T, Rokuhara A, Sakamoto Y *et al.* Sensitive enzyme immunoassay for hepatitis B virus core-related antigens and their correlation to virus load. *J Clin Microbiol* 2002; **40**: 439–45.
27 Kimura T, Rokuhara A, Matsumoto A *et al.* New enzyme immunoassay for detection of hepatitis B virus core antigen (HBcAg) and relation between levels of HBcAg and HBV DNA. *J Clin Microbiol* 2003; **41**: 1901–6.
28 Abe A, Inoue K, Tanaka T *et al.* Quantitation of hepatitis B virus genomic DNA by real-time detection PCR. *J Clin Microbiol* 1999; **37**: 2899–903.
29 Sugauchi F, Mizokami M, Orito E *et al.* A novel variant genotype C of hepatitis B virus identified in isolates from Australian Aborigines: complete genome sequence and phylogenetic relatedness. *J Gen Virol* 2001; **82** (Pt 4): 883–92.
30 Shin IT, Tanaka Y, Tateno Y, Mizokami M. Development and public release of a comprehensive hepatitis virus database. *Hepatol Res* 2008; **38**: 234–43.
31 Chisari FV, Ferrari C Hepatitis B virus immunopathogenesis. *Annu Rev Immunol* 1995; **13**: 29–60.
32 Carman WF, Jacyna MR, Hadziyannis S *et al.* Mutation preventing formation of hepatitis B e antigen in patients with chronic hepatitis B infection. *Lancet* 1989; **2** (8663): 588–91.
33 Buckwold VE, Xu Z, Chen M, Yen TS, Ou JH. Effects of a naturally occurring mutation in the hepatitis B virus basal core promoter on pre-core gene expression and viral replication. *J Virol* 1996; **70**: 5845–51.
34 Okamoto H, Tsuda F, Akahane Y *et al.* Hepatitis B virus with mutations in the core promoter for an e antigen-negative phenotype in carriers with antibody to e antigen. *J Virol* 1994; **68**: 8102–10.
35 Lamberts C, Nassal M, Velhagen I, Zentgraf H, Schroder CH. Precore-mediated inhibition of hepatitis B virus progeny DNA synthesis. *J Virol* 1993; **67**: 3756–62.
36 Chen MT, Billaud JN, Sallberg M *et al.* A function of the hepatitis B virus pre-core protein is to regulate the immune response to the core antigen. *Proc Natl Acad Sci USA* 2004; **101**: 14913–8.
37 Chen M, Sallberg M, Hughes J *et al.* Immune tolerance split between hepatitis B virus pre-core and core proteins. *J Virol* 2005; **79**: 3016–27.
38 Bocharov G, Ludewig B, Bertoletti A *et al.* Underwhelming the immune response: effect of slow virus growth on CD8+-T-lymphocyte responses. *J Virol* 2004; **78**: 2247–54.
39 Sainokami S, Abe K, Sato A *et al.* Initial load of hepatitis B virus (HBV), its changing profile, and pre-core/core promoter mutations correlate with the severity and outcome of acute HBV infection. *J Gastroenterol* 2007; **42**: 241–9.
40 Tassopoulos NC, Papaevangelou GJ, Roumeliotou-Karayannis A, Ticehurst JR, Feinstone SM, Purcell RH. Search for hepatitis B virus DNA in sera from patients with acute type B or non-A, non-B hepatitis. *J Hepatol* 1986; **2**: 410–8.

J Gastroenterol (2009) 44:733–741
DOI 10.1007/s00535-009-0053-7

ORIGINAL ARTICLE—LIVER, PANCREAS, AND BILIARY TRACT

Usefulness of Sonazoid contrast-enhanced ultrasonography for hepatocellular carcinoma: comparison with pathological diagnosis and superparamagnetic iron oxide magnetic resonance images

Keiko Korenaga · Masaaki Korenaga · Matakazu Furukawa · Takahiro Yamasaki · Isao Sakaida

Received: 16 September 2008 / Accepted: 25 February 2009 / Published online: 23 April 2009

Abstract
Objective We investigated the usefulness of Sonazoid contrast-enhanced ultrasonography (Sonazoid-CEUS) in the diagnosis of hepatocellular carcinoma (HCC). The examination was performed by comparing the images during the Kupffer phase of Sonazoid-CEUS with superparamagnetic iron oxide magnetic resonance (SPIO-MRI).
Methods The subjects were 48 HCC nodules which were histologically diagnosed (well-differentiated HCC, $n = 13$; moderately differentiated HCC, $n = 30$; poorly differentiated HCC, $n = 5$). We performed Sonazoid-CEUS and SPIO-MRI on all subjects. In the Kupffer phase of Sonazoid-CEUS, the differences in the contrast agent uptake between the tumorous and non-tumorous areas were quantified as the Kupffer phase ratio and compared. In the SPIO-MRI, it was quantified as the SPIO-intensity index. We then compared these results with the histological differentiation of HCCs.
Results The Kupffer phase ratio decreased as the HCCs became less differentiated ($P < 0.0001$; Kruskal–Wallis test). The SPIO-intensity index also decreased as HCCs became less differentiated ($P < 0.0001$). A positive correlation was found between the Kupffer phase ratio and the SPIO-MRI index ($r = 0.839$). In the Kupffer phase of Sonazoid-CEUS, all of the moderately and poorly differentiated HCCs appeared hypoechoic and were detected as a perfusion defect, whereas the majority (9 of 13 cases, 69.2%) of the well-differentiated HCCs had an isoechoic pattern. The Kupffer phase images of Sonazoid-CEUS and SPIO-MRI matched perfectly (100%) in all of the moderately and poorly differentiated HCCs.
Conclusion Sonazoid-CEUS is useful for estimating histological grading of HCCs. It is a modality that could potentially replace SPIO-MRI.

Keywords Sonazoid · Contrast-enhanced ultrasonography · Kupffer phase · SPIO-MRI · Hepatocellular carcinoma

K. Korenaga · M. Korenaga · T. Yamasaki · I. Sakaida
Department of Gastroenterology and Hepatology, Graduate School of Medicine, Yamaguchi University, 1-1-1 Minami-Kogushi, Ube, Yamaguchi 755-8505, Japan

M. Furukawa
Department of Radiology, Graduate School of Medicine, Yamaguchi University, 1-1-1 Minami-Kogushi, Ube, Yamaguchi, Japan

Present Address:
K. Korenaga (✉)
Division of Hepatology and Pancreatology, Department of Internal Medicine, Kawasaki Medical College, 577 Matsushima, Kurashiki, Okayama 702-0192, Japan
e-mail: keikore@med.kawasaki-m.ac.jp

Introduction

Ultrasonography (US) is extensively used as a diagnostic modality for hepatic focal lesions, based on their distinctive echogenicities, the gray-scale morphologic features. However, detection and characterization of tumor vascularity are important in the differential diagnosis of a liver mass. For definitive diagnosis, it has been used in combination with other contrast imaging modalities such as computer tomography (CT), magnetic resonance imaging (MRI), and angiography.

Recently, US contrast agents and novel technologies for ultrasonic imaging have been developed to improve

diagnostic ability. The first generation contrast agent Levovist (galactose 99.9%, palmitic acid 0.1%; Bayer, Osaka, Japan) is commercially available in many countries. Levovist contrast-enhanced ultrasonography (Levovist-CEUS) is considered effective for the differential diagnosis of hepatic tumors [1–3], estimation of histological malignancy [4], evaluation of effectiveness of transcatheter arterial chemoembolization [5], and guidance in percutaneous radiofrequency ablation (RFA) therapy [6, 7] for hepatocellular carcinomas (HCCs). However, Levovist microbubbles are fragile and easily collapsed by the sound pressure of ultrasound. Since ultrasound transmission is performed intermittently to avoid microbubble collapse, the real-time properties are poor during the vascular phase. Another disadvantage is the short observation time due to the instability of microbubbles during the post-vascular phase. The Kupffer imaging in the post-vascular phase can be performed by only a single sweep scan of the liver. In order to improve the contrast effects, second-generation agents that use less soluble gases for microbubbles are being developed.

Sonazoid (Daiichi-Sankyo, Tokyo, Japan; GE Healthcare, Milwaukee,WI) is a lipid-stabilized suspension of perfluorobutane. Its microbubbles are chemically stable in blood vessels [8–10], and blood flow images can be obtained in real time. In addition, Sonazoid is markedly taken up by the Kupffer cells (reticuloendothelial system components of the liver) more than Levovist [11–14]. This uniqueness of Sonazoid enhances contrast of the liver parenchyma during the post-vascular phase (i.e., Kupffer phase) [8]. The imaging in the Kupffer phase is stable from 10 to 120 min after infusion, and tolerable for multiple scanning [8]. Malignant hepatic tumors contain few or no Kupffer cells [15], which lead to clear negative contrast as a perfusion defect in the Kupffer phase. Some studies have used this property and reported on the effectiveness of Sonazoid contrast-enhanced ultrasonography (Sonazoid-CEUS) in the detection of metastatic hepatic tumors in rabbits [16], the clinical detection [17] and differentiation [18] of human hepatic tumors, and the guidance in RFA therapy for HCCs [19].

Superparamagnetic iron oxide (SPIO) is a tissue-specific MRI contrast agent, and like Sonazoid it is phagocytized by the liver Kupffer cells. SPIO-MRI imaging reflects the number of Kupffer cells and is useful in not only hepatic tumor detection but also the estimation of histological grading in HCCs [20]. Inoue et al. [4] compared the findings of Levovist-CEUS and SPIO-MRI. They found a good correlation between the findings of these methods in the delayed parenchymal-phase. However, there has not been a report comparing the diagnosability using a quantitative scale between Sonazoid-CEUS in the Kupffer phase and SPIO-MRI.

In this study, we examined the usefulness of Sonazoid-CEUS, particularly in the Kupffer phase, in HCCs diagnosis by quantifying the Sonazoid uptake and comparing the findings with those of SPIO-MRI. In addition to the detection of HCCs in the Kupffer phase, we sought to examine whether or not histological differentiation can be predicted.

Patients and methods

Patients

The subjects were 43 consecutive patients with HCCs, who were examined by both Sonazoid-CEUS and SPIO-MRI at our institution between January 2007 and April 2008. There were 30 males and 13 females and their mean age was 67 years old (range 57–80 years). Coexisting liver diseases included hepatitis C virus (HCV)-related cirrhosis in 28 patients, HCV-related chronic hepatitis in 7 patients, hepatitis B virus (HBV)-related cirrhosis in 3 patients, HBV-related chronic hepatitis in 1 patient, alcoholic cirrhosis in 2 patients, and cirrhosis of unknown etiology in 2 patients. All patients underwent an informed consent process which was approved by the ethics committee of our hospital.

Diagnosis of HCCs

Forty-eight tumors in 43 patients were detected using conventional gray-scale sonography. The mean diameter of these tumors was 2.8 cm (range 0.7–11.0 cm). All tumors were histologically diagnosed as HCCs. The diagnosis of HCCs was made by pathologists in a blind manner and according to the histological criteria of the International Working Party [21]. The pathological specimens of 29 HCC nodules were obtained from 26 patients by 21-gauge needle biopsy (Magima needle: Top, Tokyo, Japan). The pathological specimens of the remaining 19 nodules were obtained from the other 17 patients by partial hepatectomy. Of these specimens obtained from 48 HCCs, 39 were histologically uniform and 9 were composed of 2 different histological grades of HCCs (well-differentiated HCC with a minor component of moderately differentiated HCC in 2, moderately differentiated HCC with a minor component of well-differentiated HCC in 3, moderately differentiated HCC with a minor component of poorly differentiated HCC in 2, and poorly differentiated HCC with a minor component of moderately differentiated HCC in 2). HCCs with regions of varying histological grades were classified as belonging to the predominating histological characteristic. As the final diagnoses, 13 of the 48 nodules were diagnosed as well-differentiated HCCs, 30 were diagnosed as moderately differentiated HCCs, and 5 were diagnosed as poorly differentiated HCCs.

Imaging

Sonazoid-contrast enhanced US study

Contrast-enhanced sonography was performed using an ACUSON Sequoia 512 ultrasound system (Mochida Siemens Medical Systems, Tokyo). A contrast pulse sequencing (CPS) mode imaging software program was used in this contrast enhanced sonographic system. CPS technology is the latest technology which has high resolution by phase inversion and high sensitivity by power modulation. The technology can effectively extract contrast agent signals and form a highly specific and sensitive contrast display.

The CPS setup was 0.2–0.3 for the low mechanical index, −18 to −15 decibels for transmission power, 60–65 decibels for the dynamic range, and 10 frames per second for the frame rate. The focus point was established at the lower end of the lesion.

The suspension of the sonographic contrast agent Sonazoid was prepared by gently shaking and inverting Sonazoid powder and 2 ml of distilled water for 1–2 min. The suspension was allowed to stand for 1 min to homogenize. Then a Sonazoid concentration of 8 μL of microbubbles/mL was produced. The suspension was injected into the antecubital vein using a 21-gauge needle, and 0.01 ml/kg body weight of the suspension was injected manually at approximately 1 ml/s. Normal saline (10 ml) was used immediately afterward for flushing.

The tumor vessel and tumor enhancement were observed in the early vascular phase (10–30 s after the injection of the contrast agent) and in the late vascular phase (30–80 s after the injection). Then, echogenicity of the tumor was observed in the post-vascular phase (we call it the Kupffer phase) at 30 min after the contrast agent injection. The reason why we analyzed the Kupffer imaging 30 min after injection is that in some HCC nodules the contrast of the contrast agent echogenicity was not sufficient for analysis between the tumorous and non-tumorous areas at 10–20 min after injection (data not shown). The real-time images in this study were stored on the hard disk of this device. Furthermore, the images were recalled from the Cine loop memory and stored on the magnetopic disk.

We selected three images in the Kupffer phase, and measured the color signal of the regions of interest (ROIs) of the tumorous and non-tumorous areas of the liver. The software Auto-Tracking Contrast Quantification (Mochida Siemens) was used for measurements. The ROIs of the non-tumorous areas were established at sites with the same depths as the tumorous areas. The mean value of the three images at the Kupffer phase was calculated by the following formula:

Kupffer phase ratio = postcontrast echogenecity of tumorous lesion/postcontrast echogenecity of non-tumorous liver parenchyma.

We also observed tumor perfusion patterns and visually classified them as hyperechoic (Fig. 1b), isoechoic (Fig. 1d), or hypoechoic (Fig. 1f) patterns.

SPIO-enhanced MRI study

Patients underwent MRI with a 1.5-T whole-body imager (Magnetom Vision; Siemens Medical Systems, Erlangen, Germany; or Signa CV; GE Healthcare, Milwaukee, WI). MR images were obtained in the transverse plane with a phased-array coil. T2*-weighted images (TR/TE = 150/12 ms, 30° flip angle or TR/TE = 180/9–10 ms, 20° flip angle) were obtained by breath-hold gradient echo sequences. SPIO [Ferucarbotran (Resovist), Bayer, Osaka, Japan] was administered at a dose of 8 μmol of iron per kilogram of body weight. SPIO was administered as a rapid bolus using the hand injection method and was immediately followed by a saline solution flush of 15–20 mL. Post-contrast MR examination was initiated about 30 min after the SPIO administration. One of the authors read the signal intensities of the tumor and non-tumorous hepatic parenchyma directly from a monitor, using a region of interest (ROI). Visible blood vessels, bile ducts, and artifacts were carefully excluded from the ROI measurements in the hepatic parenchyma. An attempt was made to maintain a constant ROI area of approximately 1 cm^2 and the real sizes of ROI areas ranged from 0.5 to 1.0 cm^2. The mean of the three ROIs was calculated as the signal intensity of the non-tumorous hepatic parenchyma. Signal intensity was assessed in the three separate areas of the image at the level of the main portal vein, and all measured attenuation values were averaged for each phase. The signal intensity was measured in three areas: the left lobe of the liver, and the anterior segment and posterior segment of the right lobe of the liver. Circular ROIs were drawn to encompass as much of the lesion of the hepatic tumors as possible. To accurately evaluate the uptake of SPIO by the tumorous lesion, we referred to the method of Inoue et al. [4]. We calculated the relative intensity ratio of the tumorous lesion to non-tumorous hepatic parenchyma area on enhanced MR images and SPIO-enhanced MR images as follows;

Precontrast relative intensity ratio
= precontrast signal intensity of the tumorous lesion/precontrast signal intensity of the non-tumorous liver parenchyma.

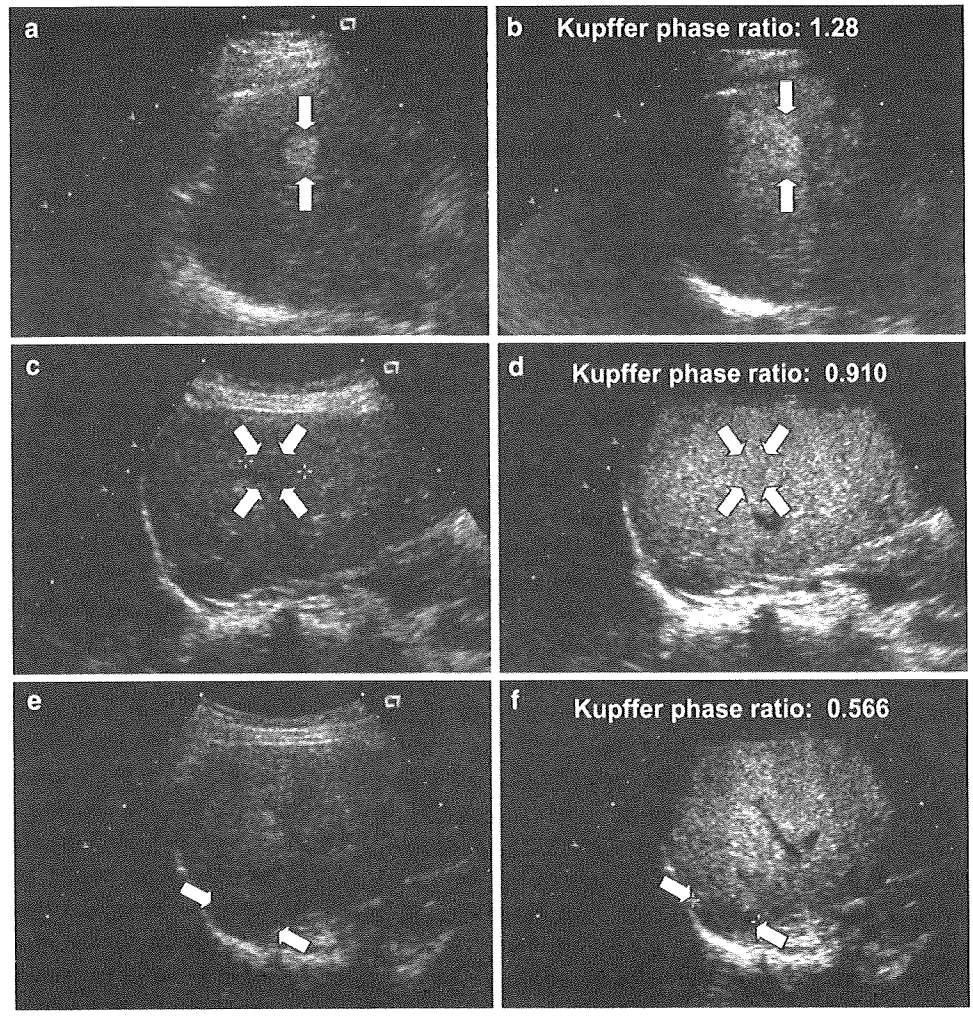

Fig. 1 Classification of the Kupffer phase findings of Sonazoid-contrast enhanced ultrasonography (Sonazoid-CEUS) in hepatocellular carcinomas (HCCs). **b** The hyper echogenecity in the Kupffer phase (*arrows*). The tumor was well-differentiated HCC and 1.5 cm in diameter on conventional harmonic gray-scale ultrasonography (US) (**a**, *arrows*). **d** The iso echogenecity in the Kupffer phase (*arrows*). The tumor was well-differentiated HCC and 2.2 cm in diameter on conventional harmonic gray scale US (**c**, *arrows*). **f** The hypo-echogenecity in the Kupffer phase, what is called "perfusion defect "(*arrows*). The tumor was moderately differentiated HCC and 2.4 cm in diameter on conventional harmonic gray-scale US (**e**, *arrows*)

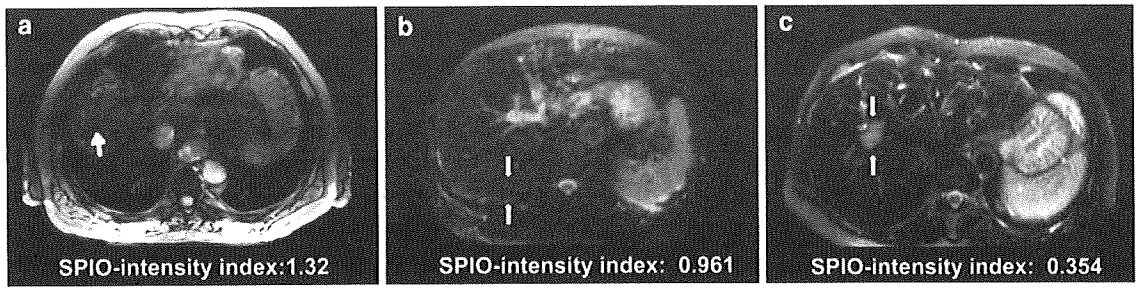

Fig. 2 Classification of the superparamagnetic iron oxide-magnetic resonance imaging (SPIO-MRI) findings in HCCs. **a** Hypointensity (*arrows*), **b** isointensity (*arrows*), **c** hyperintensity (*arrows*)

Postcontrast relative intensity ratio
= postcontrast signal intensity of the tumorous lesion/postcontrast signal intensity of the non-tumorous liver parenchyma.

We then defined the ratio of these relative intensity ratios as the SPIO intensity index, as follows;

SPIO intensity index = precontrast relativeintensity ratio/postcontrast relative intensity ratio.

We also observed the SPIO-MRI images of the tumorous tissue and visually classified them as hypo- (Fig. 2a), iso- (Fig. 2b), or hyper- (Fig. 2c) intensity.

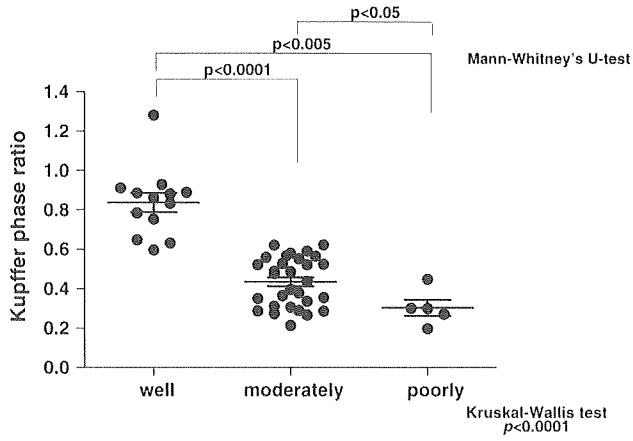

Fig. 3 Kupffer phase ratio of HCCs. The Kupffer phase ratio declined as the degree of HCCs differentiation decreased. Well-differentiated HCCs had significantly higher Kupffer phase ratio than both moderately and poorly differentiated HCCs ($P < 0.0001$ and $P < 0.005$, respectively). *Horizontal bar*, the mean of each group

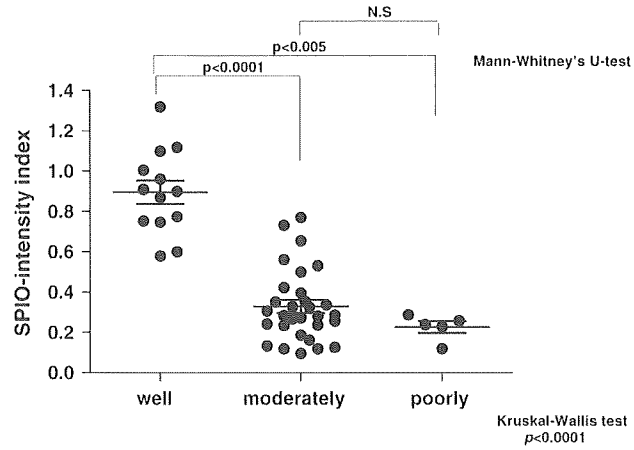

Fig. 4 SPIO intensity index of HCCs. SPIO intensity index declined as the degree of HCCs differentiation decreased. Well-differentiated HCCs had a significantly higher SPIO intensity index than both moderately and poorly differentiated HCCs ($P < 0.0001$ and $P < 0.005$, respectively). However, there was no significant difference between moderately and poorly differentiated HCCs. *Horizontal bar*, the mean of each group

Statistical analysis

The results were expressed as the mean ± SD. Statistical analysis was performed using NCSS 2007 software (Statistical Systems, Kaysville, UT). The Kruskal–Wallis test and the Mann–Whitney *U* test were used in the comparisons of the Kupffer phase ratios and SPIO-intensity indices among groups. The Pearson's coefficient of correlation was used to examine the relationship between the Kupffer phase ratio and the SPIO-intensity index. Diagnostic performance of the tests was evaluated by the receiver operating characteristic (ROC) curves from each group's quantitative measure (ratio or index).

The areas under the ROC curves (AUROCs) and 95% confidence intervals (CI) were calculated. A P value of <0.05 was established as statistically significant.

Results

Quantitative analysis of echogenicity in the Kupffer phase

Figure 3 shows the Kupffer phase ratio of HCCs. The Kupffer phase ratio declined as the HCCs became less differentiated. The mean Kupffer phase ratio was 0.836 ± 0.174 (range 0.595–1.280) for well-differentiated HCCs, 0.434 ± 0.125 (range 0.213–0.621) for moderately differentiated HCCs, and 0.303 ± 0.091 (range 0.196–0.447) for poorly differentiated HCCs, respectively. The Kupffer phase ratio was significantly greater for well-differentiated HCCs than moderately differentiated HCCs ($P < 0.0001$) or poorly differentiated HCCs ($P < 0.005$). The Kupffer phase ratio was significantly greater for moderately differentiated HCCs than poorly differentiated HCCs ($P < 0.05$).

Quantitative analysis of intensity on SPIO-MRI

Figure 4 shows the SPIO intensity index. The SPIO intensity index declined as the HCCs became less differentiated. The mean SPIO intensity index was 0.895 ± 0.211 (range 0.579–1.320) for well-differentiated HCCs, 0.329 ± 0.178 (range 0.112–0.771) for moderately differentiated HCCs, and 0.227 ± 0.065 (range 0.119–0.228) for poorly differentiated HCCs, respectively. The SPIO intensity index was significantly greater for well-differentiated HCCs than moderately differentiated HCCs ($P < 0.0001$) or poorly differentiated HCCs ($P < 0.005$). There was no significant difference in the SPIO intensity index between moderately and poorly differentiated HCCs.

Correlation between the Kupffer phase ratio and SPIO intensity index

We examined the correlation between the Kupffer phase ratio and SPIO intensity index and found a positive correlation between them ($r = 0.839$, $n = 48$, $P < 0.0001$) (Fig. 5).

Table 1 shows the findings from the images of the Kupffer phase and SPIO-MRI in the group into which moderately and poorly differentiated HCCs were merged. The images of the Kupffer phase and those of SPIO-MRI matched perfectly (100%) when these 35 HCCs were examined.

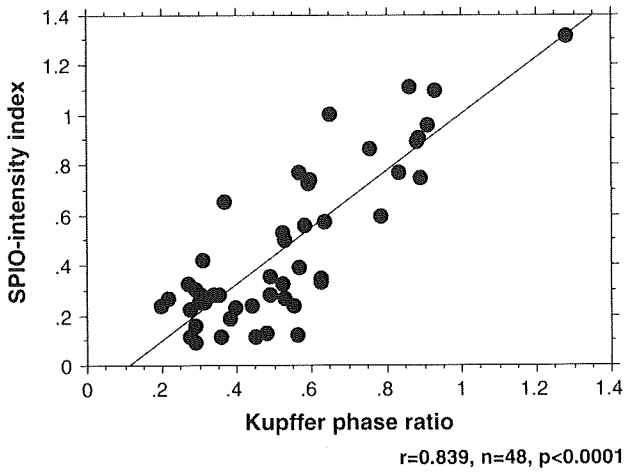

Fig. 5 Correlation between Kupffer phase ratio and SPIO intensity index for HCCs. There was a positive correlation between them ($r = 0.839$, $P < 0.001$)

Table 1 Comparison of findings in the Kupffer phase of Sonazoid contrast-enhanced ultrasonography (Sonazoid-CEUS) and in SPIO-MRI (moderately + poorly differentiated HCCs, 35 nodules)

	Kupffer phase		
	Hypo echoic	Iso echoic	Total
SPIO-MRI			
High intensity	35	0	35
Iso intensity	0	0	0
Total	35	0	35

Image consistency of the Kupffer phase and SPIO-MRI was 100% (35/35)

On the other hand, 13 of well-differentiated HCCs had a match rate of the Kupffer image and SPIO-MRI image of 69.2% (Table 2). In the well-differentiated HCCs, 3 of 13 cases (23.1%) had a hypoechoic pattern in the Kupffer phase. The majority of the well-differentiated HCCs, 9 of 13 cases (69.2%), had an isoechoic pattern. In SPIO-MRI, 5 of 13 (38.5%) cases had a decreased SPIO uptake and the images depicted as hyperintensity. There were 7 cases (53.8%) in which the images depicted as isointensity and 1 case as hypointensity (Table 2).

Comparison of the diagnostic value of Sonazoid-CEUS and SPIO-MRI in detection of moderate and poorly differentiated HCCs from well-differentiated HCCs

We examined the ability to differentiate the degree of malignancy of two groups: a well-differentiated HCCs group and a group into which moderately and poorly differentiated HCCs were merged (i.e., HCCs with high biological malignancy). We conducted a statistical examination using ROC curves for the diagnostic found that the

Table 2 Comparison of findings in the Kupffer phase of Sonazoid-CEUS and in SPIO-MRI (well-differentiated HCCs, 13 nodules)

	Kupffer phase			
	Hypo echoic	Iso echoic	Hyper echoic	Total
SPIO-MRI				
High intensity	2	3	0	5
Iso intensity	1	6	0	7
Hypo intensity	0	0	1	1
Total	3	9	1	13

Image consistency of the Kupffer phase and SPIO-MRI was 69.2% (9/13)

Table 3 Area under the receiver operating characteristic curves (AUROCs) and 95% confidence intervals (CI) for the Kupffer phase of Sonazoid-CEUS and SPIO-MRI in detection of both moderate and poorly different HCCs from well-different HCCs

Modality	AUROCs (95% CI)
Sonazoid-CEUS	0.9956 (0.9529–0.9996)
SPIO-MRI	0.9824 (0.9200–0.9962)

results of Sonazoid-CEUS in the Kupffer phase and SPIO-MRI were almost identical (Table 3). Sonazoid-CEUS in the Kupffer phase and SPIO-MRI enabled statistically the same ability to distinguish both moderately and poorly differentiated HCCs from well-differentiated HCCs.

Discussion

Sonazoid is a second-generation ultrasound contrast agent approved in Japan in January 2007 ahead of any other country in the world. Its recommended dose is 0.015 ml/kg. However, general image quality is sufficiently good at doses lower than this recommended dose [19, 22], and thus, the dose can be decreased. In addition, since Sonazoid is excreted by exhalation, it can be used in patients with renal dysfunction. It also has very few serious side effects such as allergic reactions [23], and it is a contrast agent that can be used easily in a clinical setting.

Sonazoid-CEUS has a unique Kupffer phase imaging in addition to vascular imaging, because Sonazoid microbubbles are markedly phagocytosed by the Kupffer cells. The images of the Kupffer phase provide essential information for diagnosis of a liver tumor. In clinical practice, it has been reported that Sonazoid excels in the detection of metastatic liver tumors [17] and HCCs [19]. A small liver tumor of 3 mm in diameter, which cannot be detected by conventional gray-scale ultrasonography, was depicted as a perfusion defect by contrast enhanced ultrasonography [16]. Its contrast enhancement and sensitivity are very high.

Recently, methods using the stability of Sonazoid have been reported. Numata et al. [19] detected HCCs with a low ultrasound pressure in the Kupffer phase first, and then destroyed the bubbles within and around the tumor at once with a strong sound pressure. This technique enabled to visualize tumor vessels and the enhancement for backflow into the tumor vessels and vascular spaces. Kudo et al. [22] re-administered Sonazoid into HCCs which previously showed a perfusion defect in the Kupffer phase. They devised a method called "defect re-perfusion imaging" which confirms the flow of blood into the defect. Methods using these two unique characteristics of Sonazoid can be applied to treatment guidance for recurrence or applied in the determination of effectiveness after RFA therapy. Such determination of effectiveness is difficult with methods such as conventional contrast-enhanced ultrasonography like Levovist. Sonazoid-CEUS is expected to be a breakthrough which drastically changes the diagnosis and treatment of HCCs [22].

We defined the Kupffer phase ratio as the rate of the echogenecity of tumorous lesion divided by that of non-tumorus liver parenchyma merely in the Kupffer phase. However, the difference in the Sonazoid uptake between tumorous and non-tumorous areas is not reflected precisely with this formula, because the post-contrast images obtained by CPS technology contain not only signals from the contrast agent but also tissue harmonic signals. Although these signal levels from tissue as a background seem to be very low, the Kupffer phase ratio should be calculated with consideration of the pre-contrast images as in the SPIO-MRI index. We recalculated the Kupffer phase ratio by the comparison to the pre-contrast images, in the 25 HCC nodules we could examine. There was little difference between the two results with pre-contrast images and without them (the Kupffer phase ratio with pre-contrast images: 0.439 ± 0.164; the ratio without pre-contrast images: 0.442 ± 0.164). We thus think the Kupffer phase ratio calculated with only post-contrast images could be acceptable for our study.

In this study, we showed that the Kupffer phase ratio decreased along with decreasing of HCCs differentiation, suggesting that the observations in the Kupffer phase of Sonazoid-CEUS are useful in the estimation of the differentiation of HCCs. As in the previous reports [4, 20], the SPIO intensity index also decreased with decreasing HCCs differentiation.

Inoue et al. [4] used methods similar to those used in our study. They investigated the post-vascular phase ratio to examine the differences in the contrast agent uptake between the tumorous and non-tumorous areas in the post-vascular phase of Levovist-CEUS. They compared the ratio with the SPIO intensity index with 49 liver tumors (well-differentiated HCC, $n = 20$; moderately differentiated HCC, $n = 19$; poorly differentiated HCC, $n = 1$; dysplastic nodule, $n = 9$). They found a positive correlation between the post-vascular ratio and the SPIO-intensity index. The overall image consistency of the post-vascular phase and SPIO-MRI was high at 96%. In our study, we also found a high correlation between the Kupffer phase ratio and the SPIO intensity index. And, the images of Kupffer phase and SPIO-MRI matched perfectly in both moderately and poorly differentiated HCCs. It again showed the usefulness of observations in the Kupffer phase of Sonazoid-CEUS.

Numata et al. [19] examined 108 HCC nodules that were identified as hypervascular using contrast-enhanced CT. They detected 90 (83%) HCCs using conventional US. Then, they detected an additional 15 (14%) HCCs using Sonazoid-CEUS in the Kupffer phase. The remaining 3 HCC nodules were not detected in patients even after using Sonazoid-CEUS. The reason was speculated to be due to the locations of these lesions, where the lungs and gastrointestinal gas could affect the lesion imaging.

As shown above, the observations in the Kupffer phase are outstanding for the detection of moderately and poorly differentiated HCCs. Unless the lesions exist in the blind spots of ultrasonography, it can be said that the lesions are almost always detectable by the modality of the Kupffer phase alone.

For the detection of HCCs, a combination of modalities with different principles is recommended to increase the sensitivity and specificity of diagnosis. These modalities are SPIO-MRI and contrast-enhanced multi-detector-row CT (MDCT) for hemodynamic assessment [24]. Imai et al. [25] used a combination of SPIO-MRI and contrast-enhanced MDCT for the detection of hypervascular HCCs exceeding 1.5 cm in diameter. They found that this combination resulted in almost the same diagnosability as the golden standard for HCCs diagnosis—a combination of CT during hepatic arteriography (CTHA) and CT during arterial portography (CTAP). From the results of our study, we think that SPIO-MRI with such clinical significance can be replaced by Sonazoid-CEUS.

In the well-differentiated HCCs, the image consistency of the Kupffer phase of the Sonazoid-CEUS and SPIO-MRI was not high. The images of the Kupffer phase did not correspond to the SPIO-MRI in four tumors (Table 2). All of these four tumors were hypovascular in the vascular phase of CEUS, and were under 1.5 cm in diameter: two tumors were 1.0 cm and the remaining two were 1.4 cm. The clinical characteristics of these tumors were compatible to those of well-differentiated HCCs, although the pathological diagnoses were made on biopsied specimens. We speculate on the reason of the inconsistency between the Kupffer phase of the Sonazoid-CEUS and SPIO-MRI as follows. First, this inconsistency may arise from the

differences in the contrast agent dynamics. Inoue et al. [4] reported there were two well-differentiated HCCs which showed the discrepancy between the post-vascular phase of Levovist-CEUS and SPIO-MRI. They stated that SPIO accumulates in only the Kupffer cells, but Levovist might be deposited in the sinusoids and be taken up by the Kupffer cells. Thus, the microbubbles of Levovist deposited in the tumorous blood space might be increased in some well-differentiated HCCs which possess blood spaces similar to normal sinusoids, resulting in the discrepancy. Some types of ultrasound contrast agent demonstrate contrast enhancement of liver parenchyma not through the uptake of their microbubbles by Kupffer cells but through mechanical slow down in the sinusoid [26]. Watanabe et al. [14] observed the Sonazoid microbubble dynamics in a rat liver by intravital microscopy and confocal laser scanning microscopy. They concluded that the contrast enhancement in the Kupffer phase using Sonazoid resulted because of its uptake by the Kupffer cells and not because it was present in the sinusoids. Further study might be necessary to determine whether or not this phenomenon is applicable to the patients with liver cirrhosis in which complex shunts are formed via the sinusoids. Second, the inconsistency of two images may be caused by the sensitivity as a contrast agent. Most of well-differentiated HCCs contain Kupffer cells similar in number to the surrounding non-tumorous tissues [15], and the difference in the contrast agent uptake should be small between tumorous and non-tumorous areas in either SPIO-MRI or Kupffer phase. The visual determination of this small difference could have led to the difference in findings between SPIO-MRI and the Kupffer phase shown in Table 2. We did encounter a limitation pertaining to biopsy site location and actual imaging areas, because the pathological diagnoses of the four cases which showed the image inconsistency were obtained by needle biopsy. To ensure accurate pathological diagnosis, we performed at least two needle core biopsies for each case. However, the biopsy sites and related areas of the Kupffer images and SPIO-MRI images could not be precisely correlated.

In well-differentiated HCCs, 9 of 13 cases had an isoechoic pattern in the Kupffer phase, whereas there were only 3 cases with a hypoechoic pattern. Kudo et al. [22] stated that their proposed method called "defect re-perfusion imaging" is applicable to HCCs screening occurring in liver cirrhosis with rough echogenicity in the liver, in which tumor detection is difficult by conventional US alone. This method is indeed very useful in the detection of moderately or poorly differentiated HCCs which are depicted as a perfusion defect in the Kupffer phase. However, the majority of well-differentiated HCCs lesions are depicted as isoechoic lesions in the Kupffer phase. Thus, one must keep in mind that relying only on this method can lead to overlooking well-differentiated HCCs. In our study, lesions were confirmed by conventional US in all well-differentiated HCCs with an isoechoic pattern in the Sonazoid-CEUS. Thus, we would like to emphasize not only the importance of contrast-enhanced US, but also that of basic conventional US. There have been recent reports on the usefulness of MRI using contrast agents taken up by hepatocytes such as Gd-EOB-DTPA [27] and Gd-BOPTA [28]. A combination of other modalities might be desirable in the detection of well-differentiated HCCs.

Figure 1 shows the ease of differentiation between well-differentiated HCCs and other HCCs with high biological malignancy (moderately or poorly differentiated HCCs). HCCs with a low Kupffer phase ratio value, which are clearly depicted as a perfusion defect in the Kupffer phase, can be predicted as moderately or poorly differentiated HCCs. Thus, it is possible to efficiently detect highly biologically malignant HCCs with imaging in the Kupffer phase. This finding is helpful for making decisions concerning therapeutic strategy and follow-up plans of HCCs.

We examined the ability to differentiate both moderately and poorly differentiated HCCs from well-differentiated HCCs by statistically examining the area under the ROC. We found that SPIO-MRI and Sonazoid-CEUS in the Kupffer phase were almost the same, but the Kupffer phase produced better results. Further analysis showed statistically that a cutoff value of Kupffer phase ratio was 0.6 for good sensitivity (0.917) and specificity (0.920) in distinguishing between well-differentiated HCCs and other HCCs. Figure 1 also indicates that distinguishing between well-differentiated HCCs and moderately differentiated HCCs is difficult when the Kupffer phase ratio is approximately 0.6. The determination of hypervascularity or hypovascularity of tumors is considered important in differentiating between these types of HCCs. As is well known, contrast-enhanced US is useful in the evaluation of the intratumoral hemodynamics [1, 2, 29]. In our study, all of blood flow images of the early vascular phase obtained by Sonazoid-CEUS corresponded to contrast-enhanced CT in either hypervascular or hypovascular tumors. We showed the Kupffer phase imaging is useful in predicting the histological grading of HCCs. Indeed, Sonazoid-CEUS may enable us to evaluate the biological malignancy of HCC from both intratumoral hemodynamics and reticuloendothelial function. As a benefit of Sonazoid-CEUS, the vascular phase imaging and the Kupffer phase imaging can be obtained in one series of one examination. Furthermore, the procedure can be performed more easily and with less cost than SPIO-MRI. We conclude that Sonazoid-CEUS is a useful modality that can potentially replace SPIO-enhanced MRI.

Acknowledgments We thank Masahiro Saitoh and Ritsuko Fukushima, from Mochida Siemence systems Co., Ltd., for their helpful advice and expert technical assistance.

References

1. Kudo M. Contrast harmonic imaging in the diagnosis and treatment of hepatic tumors. Tokyo: Springer; 2003.
2. Wen YL, Kudo M, Zheng RQ, Ding H, Zhou P, Minami Y, et al. Characterization of hepatic tumors: value of contrast-enhanced coded phase-inversion harmonic angio. AJR Am J Roentgenol. 2004;182:1019–26.
3. von Herbay A, Vogt C, Häussinger D. Late-phase pulse-inversion sonography using the contrast agent Levovist: differentiation between benign and malignant focal lesions of the liver. AJR Am J Roentgenol. 2002;179:1273–9.
4. Inoue T, Kudo M, Watai R, Pei Z, Kawasaki T, Minami Y, et al. Differential diagnosis of nodular lesions in cirrhotic liver by post-vascular phase contrast-enhanced US with Levovist: comparison with superparamagnetic iron oxide magnetic resonance images. J Gastroenterol. 2005;40:1139–47.
5. Minami Y, Kudo M, Kawasaki T, Kitano M, Chung H, Maekawa K, et al. Transcatheter arterial chemoembolization of hepatocellular carcinoma: usefulness of coded phase-inversion harmonic sonography. AJR Am J Roentgenol. 2003;180:703–8.
6. Numata K, Isozaki T, Ozawa Y, Sakaguchi T, Kiba T, Kubota T, et al. Percutaneous ablation therapy guided by contrast-enhanced sonography for patients with hepatocellular carcinoma. AJR Am J Roentgenol. 2003;180:143–9.
7. Minami Y, Kudo M, Chung H, Kawasaki T, Yagyu Y, Shimono T, et al. Contrast harmonic sonography-guided radiofrequency ablation therapy versus B-mode sonography in hepatocellular carcinoma: prospective randomized controlled trial. AJR Am J Roentgenol. 2007;188:489–94.
8. Watanabe R, Matsumura M, Chen CJ, Kaneda Y, Ishihara M, Fujimaki M. Gray-scale liver enhancement with Sonazoid (NC100100), a novel ultrasound contrast agent; detection of hepatic tumors in a rabbit model. Biol Pharm Bull. 2003;26:1272–7.
9. Hagen EK, Forsberg F, Aksnes AK, Merton DA, Liu JB, Tornes A, et al. Enhanced detection of blood flow in the normal canine prostate using an ultrasound contrast agent. Invest Radiol. 2000;35:118–24.
10. Yao J, Teupe C, Takeuchi M, Avelar E, Sheahan M, Connolly R, et al. Quantitative 3-dimensional contrast echocardiographic determination of myocardial mass at risk and residual infarct mass after reperfusion: experimental canine studies with intravenous contrast NC100100. J Am Soc Echocardiogr. 2000;13:570–81.
11. Yanagisawa K, Moriyasu F, Miyahara T, Yuki M, Iijima H. Phagocytosis of ultrasound contrast agent microbubbles by Kupffer cells. Ultrasound Med Biol. 2007;33:318–25.
12. Watanabe R, Matsumura M, Chen CJ, Kaneda Y, Fujimaki M. Characterization of tumor imaging with microbubble-based ultrasound contrast agent, Sonazoid, in rabbit liver. Biol Pharm Bull. 2005;28:972–7.
13. Kindberg GM, Tolleshaug H, Roos N, Skotland T. Hepatic clearance of Sonazoid perfluorobutane microbubbles by Kupffer cells does not reduce the ability of liver to phagocytose or degrade albumin microspheres. Cell Tissue Res. 2003;312:49–54.
14. Watanabe R, Matsumura M, Munemasa T, Fujimaki M, Suematsu M. Mechanism of hepatic parenchyma-specific contrast of microbubble-based contrast agent for ultrasonography: microscopic studies in rat liver. Invest Radiol. 2007;42:643–51.
15. Tanaka M, Nakashima O, Wada Y, Kage M, Kojiro M. Pathomorphological study of Kupffer cells in hepatocellular carcinoma and hyperplastic nodular lesions in the liver. Hepatology. 1996;24:807–12.
16. Forsberg F, Piccoli CW, Liu JB, Rawool NM, Merton DA, Mitchell DG, et al. Hepatic tumor detection: MR imaging and conventional US versus pulse-inversion harmonic US of NC100100 during its reticuloendothelial system-specific phase. Radiology. 2002;222:824–9.
17. Nakano H, Ishida Y, Hatakeyama T, Sakuraba K, Hayashi M, Sakurai O, et al. Contrast-enhanced intraoperative ultrasonography equipped with late Kupffer-phase image obtained by sonazoid in patients with colorectal liver metastases. World J Gastroenterol. 2008;14:3207–11.
18. Hatanaka K, Kudo M, Minami Y, Ueda T, Tatsumi C, Kitai S, et al. Differential diagnosis of hepatic tumors: value of contrast-enhanced harmonic sonography using the newly developed contrast agent, Sonazoid. Intervirology. 2008;51(Suppl 1):61–9.
19. Numata K, Morimoto M, Ogura T, Sugimori K, Takebayashi S, Okada M, et al. Ablation therapy guided by contrast-enhanced sonography with Sonazoid for hepatocellular carcinoma lesions not detected by conventional sonography. J Ultrasound Med. 2008;27:395–406.
20. Imai Y, Murakami T, Yoshida S, Nishikawa M, Ohsawa M, Tokunaga K, et al. Superparamagnetic iron oxide-enhanced magnetic resonance images of hepatocellular carcinoma: correlation with histological grading. Hepatology. 2000;32:205–12.
21. International Working Party. Terminology of nodular hepatocellular lesions. Hepatology. 1995;22:983–93.
22. Kudo M, Hatanaka K, Chung H, Minami Y, Maekawa K. A proposal of novel treatment-assist technique for hepatocellular carcinoma in the Sonazoid-enhanced ultrasonography: value of defect re-perfusion imaging. Acta Hepatol Jpn. 2007;48:299–301.
23. Moriyasu F. Phase III multicenter clinical trial of Sonazoid in Japan for the characterization and the detection of focal liver lesions. Hepatology. 2004;40(Suppl 1):707A.
24. Asahina Y, Izumi N, Uchihara M, Noguchi O, Ueda K, Inoue K, et al. Assessment of Kupffer cells by ferumoxides-enhanced MR imaging is beneficial for diagnosis of hepatocellular carcinoma: comparison of pathological diagnosis and perfusion patterns assessed by CT hepatic arteriography and CT angioportography. Hepatol Res. 2003;27:196–204.
25. Imai Y, Murakami T, Hori M, Fukuda K, Kim T, Marukawa T, et al. Hypervascular hepatocellular carcinoma: combined dynamic MDCT and SPIO-enhanced MRI versus combined CTHA and CTAP. Hepatol Res. 2008;38:147–58.
26. Kono Y, Steinbach GC, Peterson T, Schmid-Schönbein GW, Mattrey RF. Mechanism of parenchymal enhancement of the liver with a microbubble-based US contrast medium: an intravital microscopy study in rats. Radiology. 2002;224:253–7.
27. Huppertz A, Balzer T, Blakeborough A, Breuer J, Giovagnoni A, Heinz-Peer G, et al. Improved detection of focal liver lesions at MR imaging: multicenter comparison of gadoxetic acid-enhanced MR images with intraoperative findings. Radiology. 2004;230:266–75.
28. Kim SK, Kim SH, Lee WJ, Kim H, Seo JW, Choi D, et al. Preoperative detection of hepatocellular carcinoma: ferumoxides-enhanced versus mangafodipir trisodium-enhanced MR imaging. AJR Am J Roentgenol. 2002;179:741–50.
29. Giorgio A, Ferraioli G, Tarantino L, de Stefano G, Scala V, Scarano F, et al. Contrast-enhanced sonographic appearance of hepatocellular carcinoma in patients with cirrhosis: comparison with contrast-enhanced helical CT appearance. AJR Am J Roentgnol. 2004;183:1319–26.